

Continuum Modeling with Functional Lennard-Jones Parameters for Methane Storage inside Various Carbon Nanostructures

Kyle Stevens,* Ngamta Thamwattana, and Thien Tran-Duc



Cite This: *ACS Omega* 2022, 7, 29773–29786



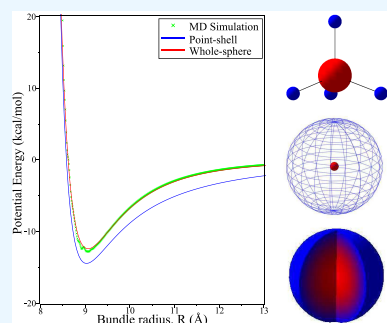
Read Online

ACCESS |

Metrics & More

Article Recommendations

ABSTRACT: Methane capture and storage are of particular importance for the development of new technology to reduce the effects of climate change and global warming. Carbon-based nanomaterials are among several porous nanomaterials proposed as potential candidates for methane storage. In this paper, we adopt a new continuum approach with functional Lennard-Jones parameters to provide interaction energies for methane inside carbon nanostructures, namely fullerenes, nanotube bundles, and nanocones. This study provides a significant improvement to previous continuum modeling approaches using the Lennard-Jones potential.



1. INTRODUCTION

Methane (CH_4) is the smallest hydrocarbon molecule, comprising one carbon and four hydrogen atoms (Figure 1a), and is well-known as one of the main greenhouse gases in

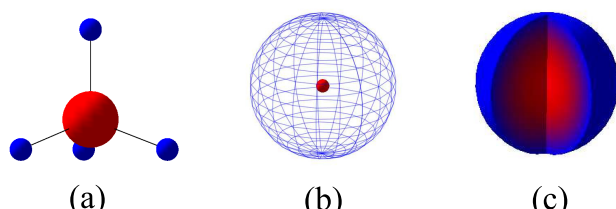


Figure 1. Three representations of methane (CH_4): (a) discrete stick-and-ball model, (b) semicontinuous (point–shell model), and (c) fully continuous heterogeneous sphere model.

the atmosphere causing global warming and climate change.^{1,2} Even though the concentration of carbon dioxide (CO_2) is much higher than that of methane in air, the effect of methane on the rising earth temperature and global warming is found to be 20–28 times higher than that of CO_2 .³ A 2021 report also shows the rapid rise of methane in the atmosphere, where methane concentration was found to have risen past 1800 ppb, tripling preindustrial levels.⁴ Capturing methane and other greenhouse gases from the atmosphere is therefore an urgent and critical task which attracts research attention worldwide. However, capturing methane from the atmosphere is very challenging due to its dilution in air, its stable C–H bond that is hard to activate,⁵ and the difficulty of separating it from nitrogen.⁶ As a result, a number of techniques have been proposed to capture methane, which include membrane

absorption,⁷ adsorption to nanoporous materials,⁸ and more advanced adsorption methods.^{9–12}

Another related area of research is methane storage. This area has also received much research interest ranging from designing and synthesizing suitable molecular containers to understanding mechanisms of adsorption and interactions between methane and potential storage structures.^{13–16} A number of porous nanomaterials have been proposed for methane storage including metal–organic frameworks, porous aromatic frameworks, covalent organic frameworks, zeolites, activated carbon, and other porous materials.^{17–21} Further, carbon-based nanomaterials are also considered as potential candidates for methane storage due to their excellent mechanical strength and chemical and thermal stability.^{22,23}

The adsorption of methane onto surfaces of carbon structures is typically governed by the physisorption mechanism.^{24–26} As the forces present in physisorption are predominantly van der Waals forces, the interactions between methane molecules and carbon structures can be evaluated using the Lennard-Jones potential²⁷

$$E = -A\rho^{-6} + B\rho^{-12} \quad (1)$$

which computes the potential energy, E , between two atoms at distance ρ apart. The coefficients A and B are the attractive and

Received: April 20, 2022

Accepted: August 1, 2022

Published: August 18, 2022



repulsive constants of the interaction, respectively. In the conventional discrete approach adopted in molecular dynamics studies, the potential energy between two molecules is simply the pairwise sum of the potentials of their constituent atoms. In order to reduce computational costs, as well as to produce mathematical expressions that are tractable and readily computable, continuous models are often adopted to replace the discrete atomic structures of the molecules.^{28–35}

In the continuum approach, atoms on the interacting molecules are assumed to be distributed, typically uniformly, over the surfaces for shell-like molecules or the volumes for dense molecules. Thus, the interaction energy can be evaluated by computing integrals of the interatomic potential over the surfaces or volumes, scaled by their atomic densities.²⁹ While this approach is suitable for homogeneous structures comprising the same type of atoms (also known as homonuclear molecules), it seems to not work well for heterogeneous, or heteronuclear, molecules, such as methane and coronene, which comprise more than one type of atoms.^{36,37} Specifically, coronene and methane comprise carbon atoms in the central region and hydrogen atoms at the perimeter. Smearing the entire surface (or volume) homogeneously implies the same interaction strength throughout the molecule, which seems counterintuitive as interactions involving hydrogen atoms are generally weaker than those involving carbon atoms. To address this shortcoming, a semicontinuous approach has been proposed that involves approximating a heteronuclear molecule by multiple homonuclear pieces. For example, benzene or coronene uses a combination of concentric rings of carbon and hydrogen atoms, where the carbon or hydrogen atoms are uniformly distributed on each ring.^{31,38} For methane, a semicontinuous approach can be thought of as a point–shell model, where the carbon atom is represented as a point centered inside a spherical shell over which the four hydrogen atoms are homogeneously smeared (see Figure 1b).

The point–shell approximation has been used to model the interactions of methane with various nanostructures, such as nanotubes³⁹ and nanotube bundles,⁴⁰ graphene,⁴¹ nanocones,⁴² and fullerenes,⁴¹ in order to investigate their adsorption properties and their potential use as methane storage. While the semicontinuous model may give a reasonable approximation for the interaction energy for small molecules, such as coronene and methane, extending the model to larger size structures is computationally expensive. To address this issue, Stevens et al.³⁶ propose a new continuum model taking into account the effect of different types of atoms in heterogeneous structures. This model considers a molecule as one continuum structure for which the interaction strengths are varied as a continuous function depending on the location and type of the atoms comprising the molecule. For the structure of methane, we assume a dense sphere (see Figure 1c) such that the interaction strength is stronger in the central region (red) due to the carbon atom and weaker toward the spherical surface (blue) due to hydrogen atoms. Accordingly, interaction functions $A(r)$ and $B(r)$ are used in place of the interaction constants (A and B) in the Lennard-Jones potential.

For methane–nanotube and coronene–nanotube interactions, Stevens et al.³⁷ demonstrate that applying a homogeneous approximation to a heterogeneous molecule can lead to inaccurate results, particularly at small intermolecular distances. Furthermore, results from Stevens et al.’s³⁶ continuous

model of methane encapsulated within a carbon nanotube show better agreement with molecular dynamics simulations than that of the semicontinuous approach used by Adisa et al.³⁹ As such, this paper applies the continuous model assuming methane as a whole sphere of varying interaction strength³⁶ to study the problems presented by Adisa et al.,^{40–42} which are methane encapsulated in a fullerene, methane within a nanotube bundle, and methane entering an open nanocone. Our aim is to provide an alternative method for energy calculations that give better agreement to molecular dynamics simulations and is less computationally expensive compared to a semicontinuous model. We comment that it is important to continue the development of a continuum approach to produce more realistic results that can be used as a guideline for experiments prior to investing in highly computational methods, such as *ab initio* and density functional theory.

In section 2, we describe the whole sphere continuum model for methane and state analytical expressions for the potential energy of methane interacting with fullerenes, nanotube bundles, and nanocones. In section 3, numerical results are presented in comparison with those obtained from molecular dynamics simulations and semicontinuous models, which we reproduce based on Adisa et al.^{40–42} Conclusions are given in section 4, and Appendix A, Appendix B, and Appendix C provide detailed derivations for the integrals K_n for the three problems. Finally, in Appendix D, we outline basic details for the molecular dynamics simulations.

2. MODELING APPROACH

In this section, we model the interactions between methane and three carbon nanostructures, namely fullerenes, nanotube bundles, and open nanocones.

Since the three carbon nanostructures comprise only carbon atoms and have shell-like structures, we approximate them as continuum surfaces where carbon atoms are uniformly distributed over their entire surfaces. For the methane molecule, we model it as a sphere of radius a . As shown in Figure 1c, the sphere has an inner core region (red) of carbon, an outer layer (blue) of hydrogen, and a transitional layer (purple) that is a blend of the two.

According to Stevens et al.,³⁷ the interaction energy E between methane and a homogeneous nanostructure can be evaluated by

$$E = \eta_1 \eta_2 (-K_3 + K_6) \quad (2)$$

where η_i is the atomic density of a given molecule in the interaction and K_n ($n = 3, 6$) is the integral defined by

$$K_n = \int_V \int_S f_n \rho^{-2n} dV dS \quad (3)$$

where ρ is the Euclidean distance between two molecules, dS is the surface element of the carbon nanostructure, and dV is the volume element of the methane molecule, which has the standard Cartesian representation $(r \sin \phi \cos \theta, r \sin \phi \sin \theta, r \cos \phi)$, where $r \in [0, 1]$, $\theta \in [0, 2\pi]$, and $\phi \in [0, \pi]$ are three variables parametrizing the sphere. The functions f_n for $n = 3$ and 6 are interaction functions representing the attractive and repulsive coefficients of the Lennard-Jones potential, respectively. The interaction functions are introduced as a smooth transition of interaction strength between the inner carbon core and the outer hydrogen region, which are treated as discrete entities in the point–shell model. Using the interaction functions has the twofold benefit of accounting for

the heteronuclear nature of methane and maintaining a fully continuous approximation of the molecule, allowing for a single expression to determine the potential energy between methane and the carbon nanostructure. As discussed in Stevens et al.,³⁷ we assume that $f_3(r) = A(r)$ and $f_6(r) = B(r)$ and that they follow a sigmoidal profile, where a stronger interaction is found in the inner region, due to the carbon–carbon interaction with the nanostructure, and a weaker interaction is toward the surface of the molecule, due to the hydrogen–carbon interaction. Here, we assume that the sigmoidal function has the form $\alpha \arctan(m(r_0 - r)) + \beta$, where α and β for $A(r)$ and $B(r)$ can be found, respectively, from the conditions $A(0) = A_{C-C}$, $A(a) = A_{C-H}$, $B(0) = B_{C-C}$, and $B(a) = B_{C-H}$, where the attractive and repulsive constants for carbon–carbon (C–C) and carbon–hydrogen (C–H) are given in Table 1. The parameters r_0 and m affect the profile of

Table 1. Numerical Values of Constants Used in This Paper

parameter	value
A_{C-C}	560.44 kcal/mol·Å ⁶
B_{C-C}	1121755.66 kcal/mol·Å ¹²
A_{C-H}	129.67 kcal/mol·Å ⁶
B_{C-H}	91727.95 kcal/mol·Å ¹²
methane radius	1.07 Å
mean volume density of methane	0.974 Å ⁻³
mean surface density of nanotube	0.382 Å ⁻²
radius of (8, 8) nanotube	5.428 Å
mean surface density of nanocone	0.382 Å ⁻²
mean surface density of C ₆₀	0.379 Å ⁻²
radius of C ₆₀	3.55 Å
mean surface density of C ₂₄₀	0.377 Å ⁻²
radius of C ₂₄₀	7.12 Å
mean surface density of C ₅₄₀	0.390 Å ⁻²
radius of C ₅₄₀	10.5 Å

the sigmoidal function such that they control the location of the inflection point and steepness of transition, respectively. Here we use $r_0 = 0.565$ and $m = 20$.³⁶ Numerical values for other constants used in our model, the semicontinuous model, and molecular dynamics simulations are given in Table 1.

2.1. Methane–Fullerene Interaction. Here we consider the interaction between a spherical fullerene of radius b interacting with a methane molecule, which is assumed to be encapsulated inside the fullerene (see Figure 2). The derivation of the interaction energy for nested spheres is similar to that of two separated spheres, as outlined in Adisa et

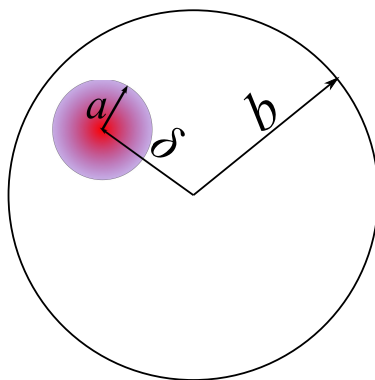


Figure 2. Diagram of methane–fullerene interaction.

al.⁴¹ However, here we have an additional radial integral to perform over the methane’s radius. Assuming the methane molecule is centered at $(0, 0, \delta)$, where δ is the distance from the center of the fullerene located at the origin, the integral K_n can be evaluated as

$$K_n = \frac{16a^3\pi^2}{b^{2n-2}} \sum_{i=0}^{\infty} \sum_{j=0}^{\lfloor i/2 \rfloor} \sum_{k=0}^{i-2j} \frac{i!(2n-1)_{2i} 2^{2j} a^{2j+2k} \delta^{2i-2j-2k}}{(2i)! (2j)! k! (i-2j-k)! (2i+1) (2j+1) b^{2i}} \int_0^1 f_n(r) r^{2+2j+2k} dr \quad (4)$$

The detailed derivation of this expression can be found in Appendix A.

2.2. Methane–Nanotube Bundle Interaction. Here we consider a methane molecule interacting with a bundle of N carbon nanotubes, each of which has radius b and is aligned parallel to and equidistant from a common axis, which we refer to as the bundle axis (see Figure 3). The perpendicular

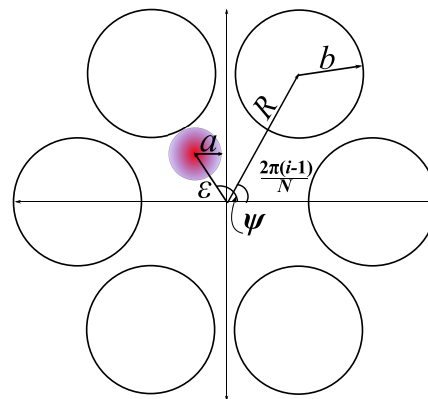


Figure 3. Diagram of methane–nanotube bundle interaction.

distance from the bundle axis to the axis of each constituent nanotube is termed the bundle radius, denoted here by R . Thus, a general point on the i th tube in the bundle is given by

$$\left(R \cos\left(\frac{2\pi(i-1)}{N}\right) + b \cos(\theta_i), R \sin\left(\frac{2\pi(i-1)}{N}\right) + b \sin(\theta_i), z_i \right)$$

where $\theta_i \in [0, 2\pi]$ and $z_i \in (-\infty, \infty)$ are variables parametrizing the i th nanotube. Here, we prescribe the coordinates for the center of the methane molecule to be $(\varepsilon \cos \psi, \varepsilon \sin \psi, 0)$, where ε is the perpendicular distance between the methane’s center and the bundle axis.

Following Adisa et al.,⁴⁰ the evaluation of the integral K_n gives

$$K_n = \frac{8\pi^3 a^3 b (2n-3)!!}{(2n-2)!!} \sum_{i=0}^{\infty} \sum_{j=0}^{\infty} \frac{\left(n - \frac{1}{2}\right)_{i+j}^2 b^{2i} (2a)^{2j}}{(i!)^2 (2j+1)! A_2^{2n+2i+2j-1}} \int_0^1 f_n(r) r^{2j+2} dr \quad (5)$$

where

$$\begin{aligned} A_2^2 &= (\epsilon \cos \psi - R \cos(2\pi(i-1)/N))^2 \\ &+ (\epsilon \sin \psi - R \sin(2\pi(i-1)/N))^2 \end{aligned} \quad (6)$$

Full derivation of this expression can be found in [Appendix B](#).

2.3. Methane–Nanocone Interaction. Here we consider the interaction of a methane molecule with an open carbon nanocone with apex angle 2ω , on which the coordinates of a typical point are given by $(z \tan \omega \cos \theta, z \tan \omega \sin \theta, z)$, where $z \in [L_1, L_2]$ and $\theta \in [0, 2\pi]$ are variables parametrizing the nanocone. As illustrated in [Figure 4](#), L_1 and L_2 are the

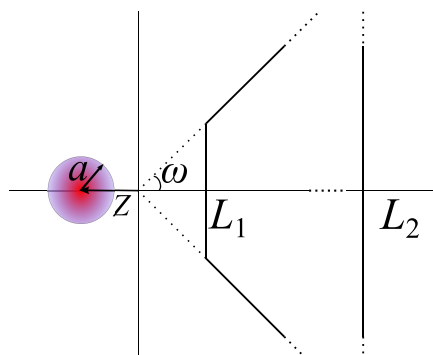


Figure 4. Diagram of methane–open nanocone interaction.

distances from the origin along the z -axis indicating the locations of the smaller and larger openings of the nanocone, respectively. For a methane molecule located at $(0, 0, Z)$, the integral K_n can be found to be a function of Z , namely

$$K_n = \frac{8\pi^2 a^3 \sin \omega}{\cos^2 \omega} \sum_{i=0}^{\infty} \frac{(n)_i \left(n - \frac{1}{2}\right)_i a^{2i}}{\left(\frac{3}{2}\right)_i i!} (I(L_2) - I(L_1)) \int_0^1 f_n(r) r^{2i+2} dr \quad (7)$$

where $I(z)$ and a detailed derivation of K_n are given in [Appendix C](#).

To evaluate K_n , we need to determine the location of the cone's smaller opening (L_1) along the z -axis and the radius at this opening. This location is critical since it is where the methane molecule is radially closest to the cone. Hence, we expect the highest interaction energy at L_1 . On the other hand, we expect a negligible interaction between methane and the cone at L_2 . This is due to the size of the methane molecule compared to the size of the opening at L_2 ; thus we use $L_2 = \infty$ to simplify the integral K_n .

Here we only consider the largest carbon nanocone with angle $\omega \approx 56.4\%$, which has been flattened as shown in [Figure 5](#). The open cone can be made by removing layers of carbon atoms from the apex located at the origin. This is equivalent to removing the atoms within the circle shown in [Figure 5](#). For example, we can remove all atoms inside the innermost circle for a small opening cone or all atoms inside the second or third circle to have a larger opening of the cone.

The circumference of these circles is given by $(5\pi/3a_0)\sqrt{n^2 + nm + m^2}$, where $(m, n) = m\vec{a} + n\vec{b}$ and a_0 is the bond length between two carbon atoms in the nanocone, taken here to be 1.42 \AA .

According to the geometry shown, L_1 is given by

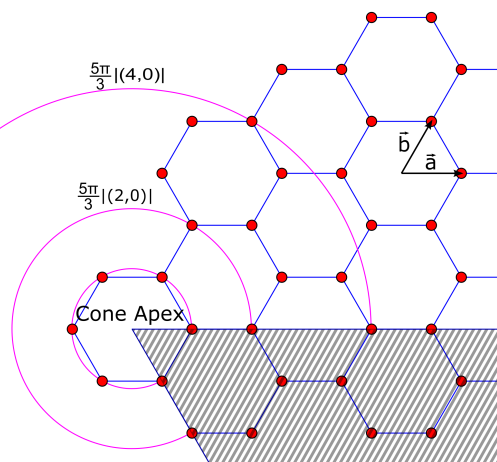


Figure 5. Flat representation of single-pentagon nanocone.

$$L_1 = \frac{5a_0}{6 \tan \omega} \sqrt{n^2 + nm + m^2}$$

We call this the “geometric” L_1 . In this paper we also consider an “adjusted” L_1 , where we extend $L_{1,\text{geom}}$ toward the origin by a certain length to account for the loss of atomic contribution at the edge of the opening. The adjusted form of L_1 is given by

$$L_{1,\text{adj}} = \sqrt{L_{1,\text{geom}}^2 - \frac{k \cos^2 \omega}{2\pi\eta_g \sin \omega}}$$

where η_g is the atomic density of graphene and k is the number of atoms found at $L_{1,\text{geom}}$. Adisa et al.⁴² present another method for determining the location of the cone's opening using the number of hexagons from the apex, K , which is given as $L_{1,\text{Adisa}} = \frac{3Ka_0 \cos \omega}{2}$.

3. RESULTS AND DISCUSSION

Here we present the interaction energy between a methane molecule and three types of carbon nanostructures, namely, (i) spherical fullerenes of various radii (C_{60} , C_{240} and C_{540}), (ii) carbon nanotube bundles comprising six $(8, 8)$ nanotubes with varying bundle radii, and (iii) open carbon nanocones with varying sizes of the smaller opening. The results obtained from our approach presented here are compared with molecular dynamics (MD) simulations (representing a fully discrete model) and those of Adisa et al.,^{39–42} which consider methane as a point of carbon atom at the center of a spherical shell of four smeared hydrogen atoms. In the following, we refer to our approach as “a whole sphere model” and that of Adisa et al.^{39–42} as “a semi-continuous model”.

All numerical evaluations for the interaction energies are performed with MAPLE, and all MD simulations are performed with LAMMPS.⁴³ As shown in this section, for a heterogeneous structure, such as methane, our improved continuum model gives excellent agreements with MD studies compared with a classical continuum approach previously used by Adisa et al.^{39–42}

(i) The potential energies for a methane molecule inside spherical fullerenes C_{60} , C_{240} , and C_{540} are shown together in [Figure 6](#). For C_{60} , the potential energy is positive for all positions of methane inside the fullerene, indicating a repulsive force between the two structures. This implies that methane cannot be encapsulated inside a C_{60} fullerene. For larger

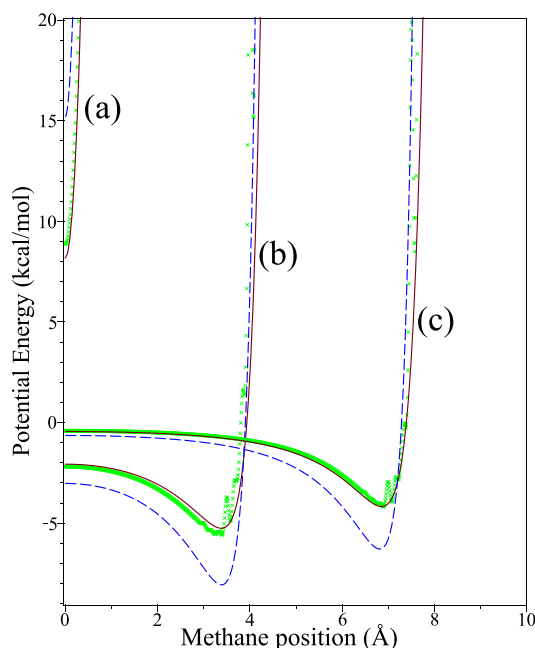


Figure 6. Comparison between energy profiles from three models for the methane–fullerene interaction with varying fullerene radii: (a) 3.55 Å (C_{60}); (b) 7.12 Å (C_{240}); (c) 10.5 Å (C_{540}). \times , simulation; —, whole sphere; --, point-shell.

fullerenes, we can see that the methane molecule can be accommodated inside C_{240} and C_{540} fullerenes due to the negative energy profile. From Figure 6, we obtain the equilibrium position of the methane molecule inside a fullerene, which is where the energy is at the minimum. It is clear that, in C_{240} and C_{540} , the methane prefers to be closer to the inner surfaces of the fullerenes rather than locating at the centers of the fullerenes. We comment that the energy profile for methane inside a fullerene is repulsive when methane is close to the inner surface of the fullerene. As shown in Figure 6, the energy rises steeply when the methane position is beyond an equilibrium position (δ_{\min}). We find that, within approximately 2 Å from the fullerene's shell, the repulsion strongly dominates the interaction.

In Table 2, we summarize the equilibrium positions (δ_{\min}) and the corresponding minimum energies (E_{\min}) for the methane molecule inside C_{240} and C_{540} fullerenes using the three approaches.

As shown in Figure 6, for all cases, results from all three approaches behave similarly. Although it is clear from Table 2 that our results from the whole sphere model give much better agreement with the simulation values compared to the semicontinuous approach. To confirm this, we benchmark

Table 2. Comparison of Results between Whole Sphere and Semicontinuous Methane Models against Simulation Values, for Varying Fullerene Radii

fullerene radius (Å)	model	δ_{\min} (Å)	E_{\min} (kcal mol ⁻¹)
7.12 (C_{240})	MD simulation	3.40	-5.598
	whole sphere	3.38	-5.258
	semicontinuous	3.39	-8.070
10.5 (C_{540})	MD simulation	6.90	-4.201
	whole sphere	6.85	-4.176
	semicontinuous	6.81	-6.289

energy results (E_{\min}) against the MD simulations and find that the absolute errors for the whole sphere model are much smaller than those for the semicontinuous model for both C_{240} and C_{540} fullerenes. For the C_{240} fullerene, the absolute errors for the whole sphere and semicontinuous models are $\epsilon_{\text{whole}} = 0.34 \text{ kcal mol}^{-1}$ and $\epsilon_{\text{semi}} = 2.472 \text{ kcal mol}^{-1}$, respectively. For the C_{540} fullerene, the absolute errors are $\epsilon_{\text{whole}} = 0.025 \text{ kcal mol}^{-1}$ and $\epsilon_{\text{semi}} = 2.088 \text{ kcal mol}^{-1}$. While the whole sphere model clearly outperforms the semicontinuous approach in determining energy minima, it is worth noting that both models perform equally well in locating the equilibrium positions. From Table 2, we can see that the absolute errors for the equilibrium positions (δ_{\min}) of methane inside C_{240} and C_{540} fullerenes are within 0.1 Å from the MD results.

We note that some significant energy fluctuations observed in the MD results presented in Figure 6 arise as the methane molecule approaches the fullerene due to effects of atomic surface roughness of the fullerene and methane molecules. This phenomenon is not seen in the continuous models since the molecules' surface is smeared out.

(ii) The methane–nanotube bundle interaction is investigated using six (8, 8) nanotubes in a bundle, with the methane molecule centered within the bundle. Figure 7 shows

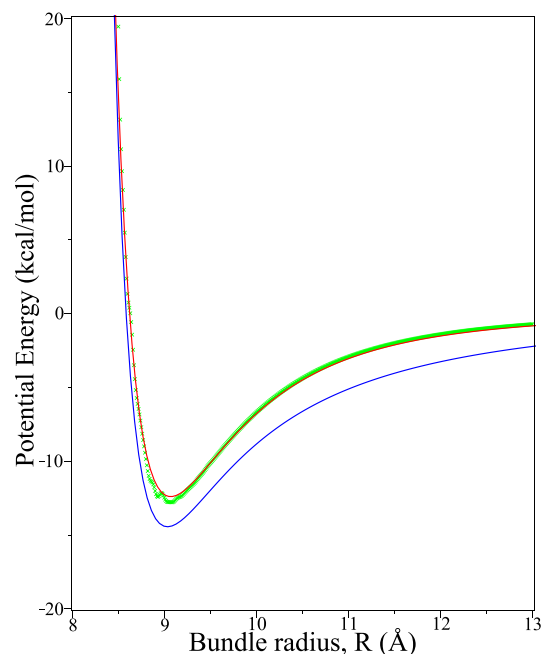


Figure 7. Comparison of energy profiles between three models for methane–nanotube bundle interaction, assuming six (8, 8) nanotubes in the bundle. Here, we fix the center of methane molecule at the origin while allowing the bundle radius R to vary. \times , simulation; red —, whole sphere; blue —, point-shell.

Table 3. Comparison of Results between Whole Sphere and Semicontinuous Models against Simulation Values for Methane inside a Bundle Comprising Six (8, 8) Nanotubes

model	R_{\min} (Å)	E_{\min} (kcal mol ⁻¹)
MD simulation	9.08	-12.808
whole sphere	9.065	-12.397
semicontinuous	9.030	-14.438

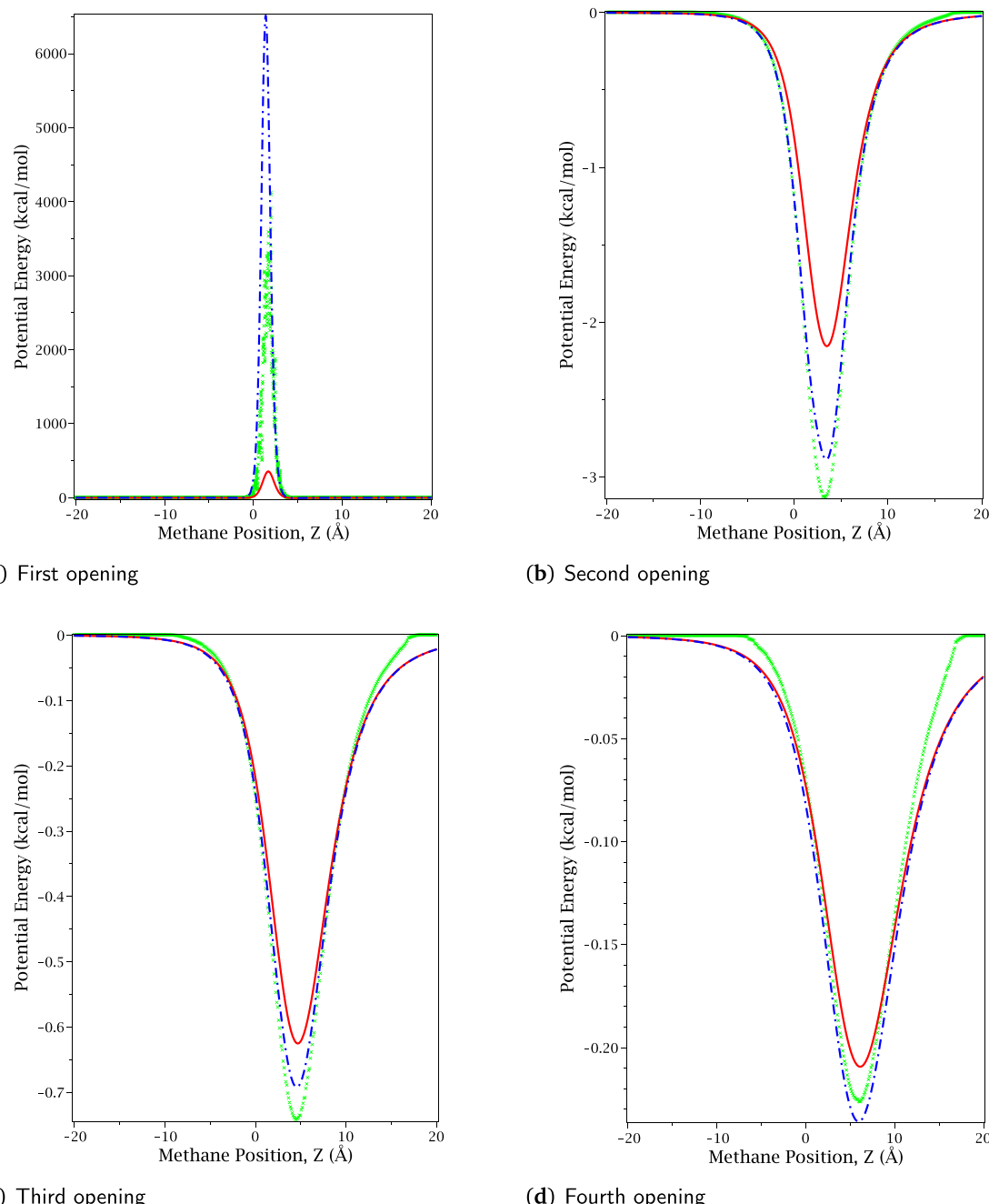


Figure 8. Energy profiles from the whole sphere model using two values of L_1 ($L_{1,\text{adj}}$ and $L_{1,\text{geom}}$). Results for all four open sizes are compared with MD simulations. \times , simulation; —, geometrically determined L_1 ; - · -, adjusted L_1 .

the energy profiles using the three approaches, and Table 3 depicts from each approach the critical bundle radius (R_{\min}) and the corresponding minimum energy (E_{\min}). Again, compared to the MD simulations, our whole sphere model outperforms the semicontinuous model. This is evident from Figure 7, which depicts excellent agreement between the whole sphere model and the MD results, whereas the semicontinuous model overestimates the potential energy for the entire interval of the bundle radius considered. Benchmarking against the MD results, we find from Table 3 that the absolute errors for E_{\min} for the whole sphere and semicontinuous models are $\epsilon_{\text{whole}} = 0.411 \text{ kcal mol}^{-1}$ and $\epsilon_{\text{semi}} = 1.63 \text{ kcal mol}^{-1}$, respectively. However, we again note that both models perform equally well in determining the critical bundle radius (R_{\min}).

(iii) The methane–nanocone interaction is investigated using a nanocone of apex angle 112.9° and various fixed opening locations (L_1) as determined in section 2. In Figure 8, we show the relationship between the potential energy and the location Z of methane along the z -axis for four different sizes of the cone’s opening at L_1 , ranging from the smallest opening (removing carbon atoms inside the first circle) to the opening that is made by removing all atoms inside the fourth circle in the geometric model (see Figure 5). Further, in Figure 8, we plot the energy using the two values of L_1 , namely $L_{1,\text{adj}}$ and $L_{1,\text{geom}}$ and compare the results with MD simulations. As shown in Figure 8, using $L_1 = L_{1,\text{adj}}$ gives results that are in closer agreement with the MD simulations for all four sizes of the openings. In addition, we note from Figure 8a that the

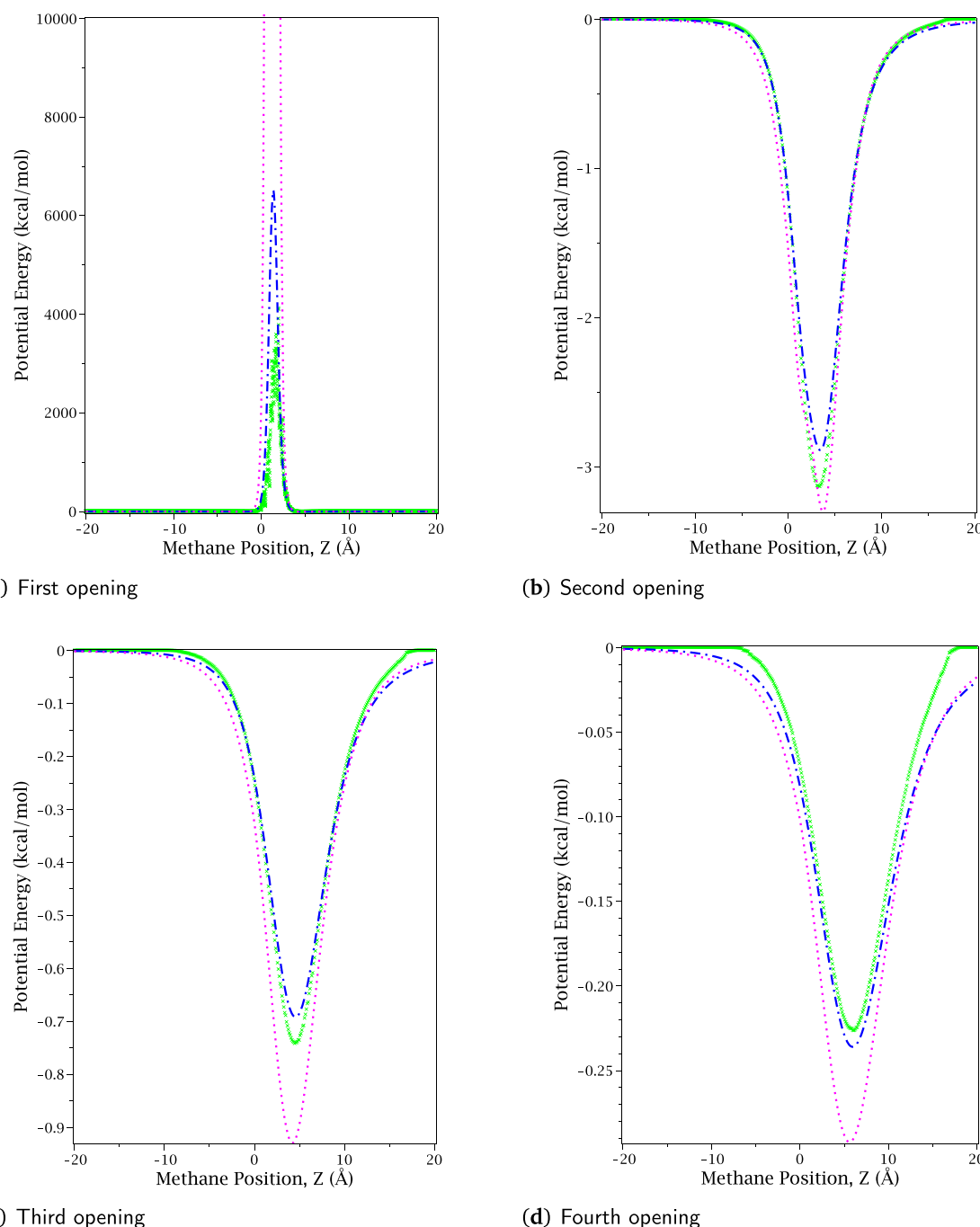


Figure 9. Comparison between energy profiles from the three approaches for the methane–nanocone interaction for four sizes of the cone opening. We note that we use $L_{1,\text{adj}}$ for the whole sphere model, while for the semicontinuous model we adopt the value $L_{1,\text{Adisa}}$ that is proposed in Adisa et al.⁴² \times , simulation; \cdots , point–shell; $- -$, whole sphere.

energy is positive (repulsive) at the opening of this cone, which implies that the methane molecule cannot enter the nanocone due to the size restriction at this opening. On the other hand, Figure 8b–d indicates the acceptance of methane inside the cones.

Using $L_{1,\text{adj}}$, we show in Figure 9 that the whole sphere model gives results that are much closer to those from the MD studies than the semicontinuous model used in Adisa et al.,⁴² especially for large sizes of the open cones. The summary of the critical location Z_{\min} and its corresponding minimum energy is given in Table 4 for all the models presented here. Using the energy results from MD simulation as a benchmark,

we obtain the absolute errors for the whole sphere model (with adjusted L_1) to be decreasing as the opening size increases: $\epsilon_{\text{whole},2} = 0.247 \text{ kcal mol}^{-1}$, $\epsilon_{\text{whole},3} = 0.05 \text{ kcal mol}^{-1}$, and $\epsilon_{\text{whole},4} = 0.009 \text{ kcal mol}^{-1}$. We note that at first the absolute error between the semicontinuous model and the MD simulation is slightly smaller than that of the whole sphere model and then becomes comparatively larger as the opening size increases: $\epsilon_{\text{semi},2} = 0.164 \text{ kcal mol}^{-1}$, $\epsilon_{\text{semi},3} = 0.187 \text{ kcal mol}^{-1}$, and $\epsilon_{\text{semi},4} = 0.065 \text{ kcal mol}^{-1}$.

We comment that the magnitudes of the potential energies for the methane–nanocone interactions (e.g., Figure 9b–d) appear to be much smaller compared to other interactions

Table 4. Comparison of Results between Whole Sphere and Semicontinuous Methane Models against Simulation Values, for Varying Sizes of the Cone Opening at L_1

opening size	model	Z_{\min} (Å)	E_{\min} (kcal mol ⁻¹)
second circle	MD simulation	3.250	-3.134
	whole sphere (geometric)	3.484	-2.154
	whole sphere (adjusted)	3.424	-2.887
	semicontinuous	3.694	-3.298
third circle	MD simulation	4.500	-0.742
	whole sphere (geometric)	4.671	-0.625
	whole sphere (adjusted)	4.556	-0.692
	semicontinuous	4.211	-0.929
fourth circle	MD simulation	6.070	-0.227
	whole sphere (geometric)	6.118	-0.209
	whole sphere (adjusted)	5.939	-0.236
	semicontinuous	5.598	-0.292

considered in this paper. This is due to the growing distance between the methane molecule and the nanocone as the methane molecule travels along the z -axis toward the cone's larger opening. Since the van der Waals forces dominate at short distances, the attraction is greater when the molecules are closer, which is the case for methane inside a fullerene and a nanotube bundle.

4. CONCLUSIONS

Carbon nanostructures have potential use for methane capture and storage. In this paper, we use a recently proposed continuum model for heterogeneous molecules to determine the interaction energies between methane and three types of carbon nanostructures. Results obtained are in closer agreement with MD simulations compared to those calculated based on a semicontinuous model used by Adisa et al.^{40–42} We comment that the difference between the fully continuous and semicontinuous models is due to the assumption made in the space between the central carbon atom and the spherical shell of hydrogen atoms, as shown in Figure 1b,c. The semicontinuous approach restricts the interaction effect of atoms to the point and the shell, while in the fully continuous model the interaction effect of the atoms in methane is distributed across the molecule. We believe that the assumption made for the fully continuous model is closer to reality as each atom's or molecule's electrons do not exist in a fixed position; hence the fully continuous model gives results that are in close agreement with MD simulations. Further, we found for each type of structure the critical distance, size, or configuration that optimizes the binding energy with methane. These findings are crucial for the development of structures for methane capture and storage. It is also clear that future modeling of gas storage involving the Lennard-Jones potential and a continuum approach should aim to include as much detail as possible within continuous structures in order to minimize deviation from the discrete case. The methods presented here can be further applied to other gases, such as CO₂, or other types of storage structures.

APPENDIX A. DERIVATION OF INTEGRAL K_N FOR METHANE–FULLERENE INTERACTION

The coordinates of a typical point on a fullerene are given by $(b \sin \phi \cos \theta, b \sin \phi \sin \theta, b \cos \phi)$, where b is the fullerene radius. The coordinates of a typical point in a methane molecule are given by $(ar \sin \sigma \cos \varphi, ar \sin \sigma \sin \varphi, ar \cos \sigma +$

$\delta)$, where δ is the distance from the center of the fullerene to the center of the methane and a is the methane's radius. The intervals over which we integrate are $r \in [0, 1]$, $\phi, \sigma \in [0, \pi]$, and $\varphi, \theta \in [0, 2\pi]$, and the surface and volume elements are $dS = b^2 \sin \phi \, d\phi \, d\theta$ and $dV = a^3 r^2 \sin \sigma \, d\varphi \, d\sigma \, dr$ for the fullerene and methane, respectively. We start with the interaction between the fullerene and an internal point located at $(0, 0, \delta)$, where δ is a distance from the origin. We denote the integral describing the interaction between the fullerene and the internal point as J_n . We then assume that the internal point is a point on the spherical methane molecule. Therefore, we can evaluate the integral J_n over the volume of the sphere, which becomes the integral K_n . This approach has been used previously when computing the entire integral between two objects is too unwieldy or intractable.²⁹

The Euclidean distance between a point on the fullerene's surface and the internal point is $\rho^2 = b^2 + \delta^2 + 2b\delta \cos \phi$. The integral J_n is written as

$$\begin{aligned} J_n &= b^2 \int_0^\pi \sin \phi \int_0^{2\pi} \frac{1}{(b^2 + \delta^2 + 2b\delta \cos \phi)^n} \\ &\quad d\theta \, d\phi \\ &= 2\pi b^2 \int_0^\pi \frac{\sin \phi}{\left((b + \delta)^2 - 4b\delta \sin^2 \frac{\phi}{2}\right)^n} \, d\phi \\ &= \frac{8\pi b^2}{(b + \delta)^{2n}} \int_0^{\pi/2} \frac{\sin \phi \cos \phi}{\left(1 - \frac{4b\delta}{(b + \delta)^2} \sin^2 \phi\right)^n} \, d\phi \end{aligned} \quad (8)$$

This integral is now in the form of eq 3.681.1 in Gradshteyn and Ryzhik;⁴⁴ thus we write eq 8 as

$$J_n = \frac{4\pi b^2}{b^{2n} \left(1 + \frac{\delta}{b}\right)^{2n}} {}_2F_1\left(n, 1; 2; \frac{4\frac{\delta}{b}}{\left(1 + \frac{\delta}{b}\right)^2}\right) \quad (9)$$

Using eq 9.134.3 in ref 44, we transform the hypergeometric function in eq 9 and expand it to arrive at

$$J_n = \frac{4\pi}{b^{2n-2}} \sum_{i=0}^{\infty} \frac{(n)_i \left(n - \frac{1}{2}\right)_i}{\left(\frac{3}{2}\right)_i i!} \left(\frac{\delta}{b}\right)^{2i} \quad (10)$$

Next, we integrate this expression over the volume of a methane molecule centered at $(0, 0, \delta)$; thus we replace the distance δ in eq 10 with the distance between the center of the fullerene and a general point within the methane molecule, $\rho^2 = a^2 r^2 + \delta^2 + 2ar\delta \cos \sigma$:

$$\begin{aligned}
K_n &= \int_0^1 \int_0^\pi \int_0^{2\pi} a^3 r^2 f_n(r) \sin \sigma J_n(\rho) d\varphi d\sigma dr \\
&= a^3 \int_0^1 f_n(r) r^2 \int_0^\pi \sin \sigma \int_0^{2\pi} \frac{4\pi}{b^{2n-2}} \\
&\sum_{i=0}^{\infty} \frac{(n)_i \left(n - \frac{1}{2}\right)_i}{\left(\frac{3}{2}\right)_i i!} \left(\frac{\rho}{b}\right)^{2i} d\varphi d\sigma dr = \frac{8a^3 \pi^2}{b^{2n-2}} \\
&\sum_{i=0}^{\infty} \frac{(n)_i \left(n - \frac{1}{2}\right)_i}{\left(\frac{3}{2}\right)_i i! b^{2i}} \int_0^1 f_n(r) r^2 \\
&\int_0^\pi \sin \sigma (a^2 r^2 + \delta^2 + 2ar\delta \cos \sigma)^i d\sigma dr \\
&= \frac{8a^3 \pi^2}{b^{2n-2}} \sum_{i=0}^{\infty} \frac{(n)_i \left(n - \frac{1}{2}\right)_i}{\left(\frac{3}{2}\right)_i i! b^{2i}} I
\end{aligned} \tag{11}$$

For brevity, we compute the integral I in eq 11 and then substitute it back into the expression at the end. As the expression for ρ is raised to a positive integer, we make use of binomial expansion to compute the integral:

$$\begin{aligned}
I &= \int_0^1 f_n(r) r^2 \int_0^\pi \sin \sigma (a^2 r^2 + \delta^2 + 2ar\delta \cos \sigma)^i d\sigma dr \\
&= \sum_{j=0}^i \frac{i!(2a\delta)^j}{j!(i-j)!} \int_0^1 f_n(r) r^{2+2j} (a^2 r^2 + \delta^2)^{i-j} \int_0^\pi \sin \sigma \cos^j \sigma d\sigma \\
&\quad dr
\end{aligned} \tag{12}$$

Here we note that

$$\int_0^\pi \sin x \cos^m x dx = \begin{cases} 2 \int_0^{\pi/2} \cos x \sin^m x dx, & m \text{ even} \\ 0, & m \text{ odd} \end{cases}$$

so we split the above sum into odd and even parts and arrive at

$$\begin{aligned}
I &= 2 \sum_{j=0}^{\lfloor i/2 \rfloor} \frac{i!(2a\delta)^{2j}}{(2j)!(i-2j)!} \int_0^1 f_n(r) r^{2+2j} (a^2 r^2 + \delta^2)^{i-2j} \\
&\quad \int_0^{\pi/2} \cos \sigma \sin^{2j} \sigma d\sigma dr = 2 \\
&\quad \sum_{j=0}^{\lfloor i/2 \rfloor} \frac{i!(2a\delta)^{2j}}{(2j)!(i-2j)!(2j+1)} \\
&\quad \int_0^1 f_n(r) r^{2+2j} (a^2 r^2 + \delta^2)^{i-2j} dr
\end{aligned} \tag{13}$$

as

$$\int_0^{\pi/2} \sin^{\mu-1} x \cos^{\nu-1} x dx = \frac{1}{2} B\left(\frac{\mu}{2}, \frac{\nu}{2}\right)$$

by eq 3.621.5 in ref 44. Now we expand the next binomial to arrive at the final expression for the integral I with the r integral reduces to the form $\int_0^1 f(r) r^\lambda dr$:

$$\begin{aligned}
I &= 2 \sum_{j=0}^{\lfloor i/2 \rfloor} \frac{i!(2a\delta)^{2j}}{(2j)!(i-2j)!(2j+1)} \int_0^1 f_n(r) r^{2+2j} \\
&\quad \sum_{k=0}^{i-2j} \frac{(i-2j)!}{k!(i-2j-k)!} (a^2 r^2)^k (\delta^2)^{i-2j-k} dr \\
&= 2 \sum_{j=0}^{\lfloor i/2 \rfloor} \sum_{k=0}^{i-2j} \frac{i! 2^{2j} a^{2j+2k} \delta^{2i-2j-2k}}{(2j)! k! (i-2j-k)! (2j+1)} \\
&\quad \int_0^1 f_n(r) r^{2+2j+2k} dr
\end{aligned} \tag{14}$$

Substituting eq 14 back into eq 11 and simplifying, we arrive at the final expression:

$$\begin{aligned}
K_n &= \frac{16a^3 \pi^2}{b^{2n-2}} \\
&\quad \sum_{i=0}^{\infty} \sum_{j=0}^{\lfloor i/2 \rfloor} \sum_{k=0}^{i-2j} \frac{i!(2n-1)_{2i} 2^{2j} a^{2j+2k} \delta^{2i-2j-2k}}{(2i)! (2j)! k! (i-2j-k)! (2i+1) (2j+1) b^{2i}} \\
&\quad \int_0^1 f_n(r) r^{2+2j+2k} dr
\end{aligned} \tag{15}$$

We have previously computed the integrals of the form $\int_0^1 f_n(x) x^k dx$ in the appendix of Stevens et al.,³⁶ so applying those for the specified f_n in eq 15, the integral K_n is now completed.

APPENDIX B. DERIVATION OF INTEGRAL K_N FOR METHANE–NANOTUBE BUNDLE INTERACTION

The coordinates of a typical point on the i th nanotube in an N -nanotube bundle centered on the origin, parallel to the z -axis, are given by

$$\begin{pmatrix} R \cos\left(\frac{2\pi(i-1)}{N}\right) + b \cos(\theta_i), \\ R \sin\left(\frac{2\pi(i-1)}{N}\right) + b \sin(\theta_i), \\ z_i \end{pmatrix}$$

where R is the bundle radius and b is the nanotube radius. The coordinates of a typical point in a methane molecule are given by $(ar \sin \phi \cos \varphi + \epsilon \cos \psi, ar \sin \phi \sin \varphi + \epsilon \sin \psi, ar \cos \varphi)$, where ϵ is the distance from the origin and a is the methane's radius. The intervals over which we integrate are $r \in [0, 1]$, $z \in (-\infty, \infty)$, $\phi \in [0, \pi]$, $\varphi \in [0, 2\pi]$, and the surface and volume elements are $dS = b dz d\theta$ and $dV = a^3 r^2 \sin \phi d\varphi d\phi dr$ for the nanotube and methane, respectively.

Let $\tau = \frac{2\pi(i-1)}{N}$; the interaction integral between the methane and the i th tube in the bundle can be written as

$$K_n = a^3 b \int_0^1 f_n(r) r^2 \int_0^\pi \sin \phi \int_0^{2\pi} \int_{-\infty}^\infty \rho^{-2n} dz d\theta d\varphi d\phi dr \tag{16}$$

where

$$\begin{aligned}
\rho^2 &= (ar \sin \phi \cos \varphi + \epsilon \cos \psi - R \cos(\tau) - b \cos(\theta))^2 \\
&+ (ar \sin \phi \sin \varphi + \epsilon \sin \psi - R \sin(\tau) - b \sin(\theta))^2 \\
&+ (z - ar \cos \varphi)^2 \\
&= A + (z - ar \cos \varphi)^2
\end{aligned} \tag{17}$$

Here, we make the substitution $z = ar \cos \varphi = A^{1/2} \tan \omega$, which gives $dz = A^{1/2} \sec^2 \omega d\omega$. The limits of integration are transformed as such that $z \in (-\infty, \infty) \Rightarrow \omega \in \left[-\frac{\pi}{2}, \frac{\pi}{2}\right]$. Applying this substitution, eq 16 becomes

$$\begin{aligned} K_n &= a^3 b \int_0^1 f_n(r) r^2 \int_0^\pi \sin \phi \int_0^{2\pi} \int_0^{2\pi} \frac{1}{A^{n-1/2}} \\ &\quad \int_{-\pi/2}^{\pi/2} \cos^{2n-2} \omega d\omega d\theta d\varphi d\phi dr = \frac{\pi a^3 b (2n-3)!!}{(2n-2)!!} \\ &\quad \int_0^1 f_n(r) r^2 \int_0^\pi \sin \phi \int_0^{2\pi} \\ &\quad \int_0^{2\pi} \frac{1}{A^{n-1/2}} d\theta d\varphi d\phi dr \end{aligned} \quad (18)$$

where $(m)!! = m(m-2)(m-4)\dots$ is the double factorial.

Regarding the expression for A , we have

$$\begin{aligned} A &= (ar \sin \phi \cos \varphi - b \cos(\theta) + \lambda_c)^2 \\ &\quad + (ar \sin \phi \sin \varphi - b \sin(\theta) + \lambda_s)^2 \end{aligned} \quad (19)$$

where $\lambda_c = \varepsilon \cos \psi - R \cos(\tau)$ and $\lambda_s = \varepsilon \sin \psi - R \sin(\tau)$. Then, we expand A to isolate the functions in θ , adding the two cosines using phasor addition:

$$\begin{aligned} A &= (ar \sin \phi \cos \varphi + \lambda_c)^2 + 2b(ar \sin \phi \cos \varphi + \lambda_c) \\ &\quad \cos(\theta - \pi) + b^2 \cos^2 \theta + (ar \sin \phi \sin \varphi + \lambda_s)^2 \\ &\quad + 2b(ar \sin \phi \sin \varphi + \lambda_s) \cos\left(\theta + \frac{\pi}{2}\right) + b^2 \sin^2 \theta \\ &= b^2 + A_1^2 + 2bA_1 \cos(\theta + \theta_1) \end{aligned} \quad (20)$$

where

$$A_1^2 = (ar \sin \phi \cos \varphi + \lambda_c)^2 + (ar \sin \phi \sin \varphi + \lambda_s)^2$$

and

$$\theta_1 = \arctan\left(\frac{ar \sin \phi \sin \varphi + \lambda_s}{-ar \sin \phi \cos \varphi - \lambda_c}\right)$$

Due to the periodicity of the integrand in θ , the limits of integration are shifted as $\int_0^{2\pi} \Rightarrow \int_{\theta_1}^{2\pi+\theta_1}$, then the linear substitution of $\theta = \theta + \theta_1$ is applied, and thus eq 18 is written as

$$\begin{aligned} K_n &= \frac{\pi a^3 b (2n-3)!!}{(2n-2)!!} \int_0^1 f_n(r) r^2 \int_0^\pi \sin \phi \\ &\quad \int_0^{2\pi} \int_0^{2\pi} \frac{1}{(b^2 + A_1^2 + 2bA_1 \cos \theta)^{n-1/2}} d\theta d\varphi d\phi dr \\ &= \frac{4\pi a^3 b (2n-3)!!}{(2n-2)!!} \int_0^1 f_n(r) r^2 \int_0^\pi \sin \phi \\ &\quad \int_0^{2\pi} \frac{1}{(b + A_1)^{2n-1}} \int_0^{\pi/2} \frac{1}{\left(1 - \frac{4bA_1}{(b+A_1)^2} \sin^2 \theta\right)^{n-1/2}} \\ &\quad d\theta d\varphi d\phi dr \end{aligned} \quad (21)$$

This is a standard form for the hypergeometric function

$${}_2F_1(\alpha, \beta; \gamma; z) = \sum_{i=0}^{\infty} \frac{(\alpha)_i (\beta)_i}{(\gamma)_i i!} z^i$$

($|z| < 1$), where $(k)_i = \frac{\Gamma(k+i)}{\Gamma(k)}$ is the Pochhammer function, also known as the rising factorial. Equation 3.681.1 in ref 44 has

$$\begin{aligned} &\int_0^{\pi/2} \frac{\sin^{2\mu-1} x \cos^{2\nu-1} x}{(1 - k^2 \sin^2 x)^\rho} dx \\ &= \frac{B(\mu, \nu)}{2} {}_2F_1(\rho, \mu; \mu + \nu; k^2) \end{aligned}$$

which is used in eq 21 to arrive at

$$\begin{aligned} K_n &= \frac{2\pi^2 a^3 b (2n-3)!!}{(2n-2)!!} \int_0^1 f_n(r) r^2 \\ &\quad \int_0^\pi \sin \phi \int_0^{2\pi} \frac{1}{A_1^{2n-1} \left(1 + \frac{b}{A_1}\right)^{2n-1}} {}_2F_1 \\ &\quad \left(n - \frac{1}{2}, \frac{1}{2}; 1; \frac{4 \frac{b}{A_1}}{\left(1 + \frac{b}{A_1}\right)^2}\right) d\varphi d\phi dr \end{aligned} \quad (22)$$

Next, the transformation

$$\begin{aligned} {}_2F_1\left(\alpha, \beta; 2\beta; \frac{4z}{(1+z)^2}\right) \\ = (1+z)^{2\alpha} {}_2F_1\left(\alpha, \alpha + \frac{1}{2} - \beta; \beta + \frac{1}{2}; z^2\right) \end{aligned}$$

is used as given in eq 9.134.3 in ref 44. Then K_n is expanded by using a hypergeometric series as

$$\begin{aligned} K_n &= \frac{2\pi^2 a^3 b (2n-3)!!}{(2n-2)!!} \int_0^1 f_n(r) r^2 \\ &\quad \int_0^\pi \sin \phi \int_0^{2\pi} \frac{\left(1 + \frac{b}{A_1}\right)^{2n-1}}{A_1^{2n-1} \left(1 + \frac{b}{A_1}\right)^{2n-1}} {}_2F_1 \\ &\quad \left(n - \frac{1}{2}, n - \frac{1}{2}; 1; \left(\frac{b}{A_1}\right)^2\right) d\varphi d\phi dr \\ &= \frac{2\pi^2 a^3 b (2n-3)!!}{(2n-2)!!} \sum_{i=0}^{\infty} \frac{\left(n - \frac{1}{2}\right)_i^{2i}}{(i!)^2} \int_0^1 f_n(r) r^2 \\ &\quad \int_0^\pi \sin \phi \int_0^{2\pi} \frac{1}{(A_1^{2i})^{n-i-\frac{1}{2}}} d\varphi d\phi dr \end{aligned} \quad (23)$$

Note that we can make the substitution with A_1/b , though this may result in convergence issues with the hypergeometric function as $A_1 \geq b$, due to the constraints of the problem. For brevity, the integrals in φ and ϕ are computed separately and then reintroduced back into eq 23, namely

$$I = \int_0^\pi \sin \phi \int_0^{2\pi} \frac{1}{((ar \sin \phi \cos \varphi + \lambda_c)^2 + (ar \sin \phi \sin \varphi + \lambda_s)^2)^{n+i-1/2}} d\varphi d\phi \quad (24)$$

Expanding the binomials in eq 24

$$\begin{aligned} A_1^2 &= (ar \sin \phi \cos \varphi + \lambda_c)^2 + (ar \sin \phi \sin \varphi + \lambda_s)^2 \\ &= a^2 r^2 \sin^2 \phi + \lambda_c^2 + \lambda_s^2 \\ &\quad + 2ar \sin \phi (\lambda_c \cos \varphi + \lambda_s \sin \varphi) \\ &= a^2 r^2 \sin^2 \phi + A_2^2 + 2ar \sin \phi A_2 \cos(\varphi + \varphi_2) \end{aligned} \quad (25)$$

where $A_2^2 = \lambda_c^2 + \lambda_s^2$ and $\varphi_2 = \arctan\left(\frac{-\lambda_s}{\lambda_c}\right)$. As the interval of integration is $[0, 2\pi]$, the same technique applied in eq 21 with the θ integral is used here in eq 24 to arrive at

$$\begin{aligned} I &= \int_0^\pi \sin \phi \int_0^{2\pi} \frac{1}{(a^2 r^2 \sin^2 \phi + A_2^2 + 2ar \sin \phi A_2 \cos \varphi)^{n+i-1/2}} d\varphi d\phi \\ &= 2 \int_0^\pi \sin \phi \int_0^{2\pi} \frac{1}{((ar \sin \phi + A_2)^2 - 4ar \sin \phi A_2 \sin^2 \frac{\varphi}{2})^{n+i-1/2}} d\varphi d\phi \quad (26) \\ &= 4 \int_0^\pi \frac{\sin \phi}{(ar \sin \phi + A_2)^{2n+2i-1}} \int_0^{\pi/2} \frac{1}{\left(1 - \frac{4ar \sin \phi A_2}{(ar \sin \phi + A_2)^2} \sin^2 \varphi\right)^{n+i-1/2}} d\varphi d\phi \end{aligned}$$

The φ integral in eq 26 is the same form for a hypergeometric function as the θ integral in eq 21; thus we make the substitution and eq 26 becomes

$$\begin{aligned} I &= 2 \int_0^\pi \frac{\sin \phi B\left(\frac{1}{2}, \frac{1}{2}\right)}{(ar \sin \phi + A_2)^{2n+2i-1}} {}_2F_1\left(n + i - \frac{1}{2}, \frac{1}{2}; 1; \frac{4ar \sin \phi A_2}{(ar \sin \phi + A_2)^2}\right) d\phi \\ &= 2\pi \int_0^\pi \frac{\sin \phi \left(1 + \frac{ar \sin \phi}{A_2}\right)^{2n+2i-1}}{A_2^{2n+2i-1} \left(1 + \frac{ar \sin \phi}{A_2}\right)^{2n+2i-1}} {}_2F_1\left(n + i - \frac{1}{2}, n + i - \frac{1}{2}; 1; \left(\frac{ar \sin \phi}{A_2}\right)^2\right) d\phi \\ &= \frac{2\pi}{A_2^{2n+2i-1}} \sum_{j=0}^{\infty} \frac{\left(n + i - \frac{1}{2}\right)_j^2 a^{2j} r^{2j}}{(j!)^2 A_2^{2j}} \int_0^\pi \sin^{2j+1} \phi d\phi \quad (27) \end{aligned}$$

Here

$$\int_0^\pi \sin^{2j+1} \phi d\phi = 2 \int_0^{\pi/2} \sin^{2j+1} \phi d\phi = \frac{(2j)!!}{(2j+1)!!}$$

Thus eq 27 simplifies to

$$I = \frac{4\pi}{A_2^{2n+2i-1}} \sum_{j=0}^{\infty} \frac{\left(n + i - \frac{1}{2}\right)_j^2 a^{2j} r^{2j} (2j)!!}{(j!)^2 A_2^{2j} (2j+1)!!} \quad (28)$$

Substituting eq 28 back into eq 23 and simplifying, we obtain the final expression for K_n with only the integral in r to be performed, namely

$$\begin{aligned} K_n &= \frac{8\pi^3 a^3 b (2n-3)!!}{(2n-2)!!} \\ &\quad \sum_{i=0}^{\infty} \sum_{j=0}^{\infty} \frac{\left(n - \frac{1}{2}\right)_{i+j}^2 b^{2i} (2a)^{2j}}{(i!)^2 (2j+1)! A_2^{2n+2i+2j-1}} \int_0^1 f_n(r) r^{2j+2} dr \end{aligned} \quad (29)$$

We note that the integral in r is computed as shown in the appendix of Stevens et al.³⁶

APPENDIX C. DERIVATION OF INTEGRAL K_N FOR METHANE–NANOCONE INTERACTION

The coordinates of a typical point on an open nanocone are given by $(z \tan \omega \cos \theta, z \tan \omega \sin \theta, z)$, where ω is half the angle at the apex of the cone. The coordinates of a typical point in a methane molecule centered on the z -axis and at a distance Z from the origin are given by $(ar \sin \phi \cos \varphi, ar \sin \phi \sin \varphi, ar \cos \phi + Z)$, where a is the methane's radius. The intervals over which we integrate are $r \in [0, 1]$, $\phi \in [0, \pi]$, and $\varphi, \theta \in [0, 2\pi]$, and the surface and volume elements are $dS = z \tan \omega \sec \omega d\theta dz$ and $dV = a^3 r^2 \sin \sigma d\varphi d\sigma dr$ for the cone and methane, respectively. We start with the interaction between the methane and point $(0, 0, \delta)$ located at a distance δ from the origin along the z -axis.

The interaction integral between the methane and the point is given by

$$J_n = a^3 \int_0^1 f_n(r) r^2 \int_0^\pi \sin \phi \int_0^{2\pi} \rho^{-2n} d\varphi d\phi dr \quad (30)$$

where

$$\begin{aligned} \rho^2 &= (ar \sin \phi \cos \varphi)^2 + (ar \sin \phi \sin \varphi)^2 \\ &\quad + (ar \cos \phi + Z - \delta)^2 = (ar + d)^2 - 4ard \sin^2 \frac{\phi}{2} \end{aligned}$$

$d = Z - \delta$. As there is no φ term in the integrand, eq 30 simplifies to

$$\begin{aligned} J_n &= 4\pi a^3 \int_0^1 f_n(r) r^2 \int_0^{\pi/2} \frac{\sin 2\phi}{((ar + d)^2 - 4ard \sin^2 \phi)^n} d\phi dr \\ &= 8\pi a^3 \int_0^1 \frac{f_n(r) r^2}{(ar + d)^{2n}} \int_0^{\pi/2} \frac{\sin \phi \cos \phi}{\left(1 - \frac{4ard}{(ar + d)^2} \sin^2 \phi\right)^n} d\phi dr \end{aligned} \quad (31)$$

which is in the form of an integral representation of the hypergeometric function (eq 3.681.1 in ref 44)

$$\int_0^{\pi/2} \frac{\sin^{2\mu-1} x \cos^{2\nu-1} x}{(1 - k^2 \sin^2 x)^\rho} dx \\ = \frac{B(\mu, \nu)}{2} {}_2F_1(\rho, \mu; \mu + \nu; k^2)$$

Thus, eq 31 is now given as

$$J_n = \frac{4\pi a^3}{d^{2n}} \int_0^1 \frac{f_n(r)r^2}{\left(1 + \frac{ar}{d}\right)^{2n}} {}_2F_1\left(n, 1; 2; \frac{4\frac{ar}{d}}{\left(1 + \frac{ar}{d}\right)^2}\right) dr \quad (32)$$

Now, we apply the transformation detailed in eq 9.134.3 in ref 44

$${}_2F_1\left(\alpha, \beta; 2\beta; \frac{4z}{(1+z)^2}\right) \\ = (1+z)^{2\alpha} {}_2F_1\left(\alpha, \alpha + \frac{1}{2} - \beta; \beta + \frac{1}{2}; z^2\right)$$

and expand the hypergeometric function

$$J_n = 4\pi a^3 \sum_{i=0}^{\infty} \frac{(n)_i \left(n - \frac{1}{2}\right)_i a^{2i}}{\left(\frac{3}{2}\right)_i i! d^{2i+2n}} \int_0^1 f_n(r) r^{2i+2} dr \quad (33)$$

Next we expand the point on the z -axis above into a cone whose central axis lies on the z -axis. We integrate over eq 33 to obtain an integral for the methane–cone interaction as

$$K_n = \int_{L_1}^{L_2} \int_0^{2\pi} z \tan \omega \sec \omega J_n(p) d\theta dz \quad (34)$$

where $p^2 = z^2 \tan^2 \omega + (z - Z)^2$ is the distance between a point on the cone and the center of the methane molecule. We substitute d for p in eq 33, which gives eq 34 the form

$$K_n = 4\pi a^3 \tan \omega \sec \omega \sum_{i=0}^{\infty} \frac{(n)_i \left(n - \frac{1}{2}\right)_i a^{2i}}{\left(\frac{3}{2}\right)_i i!} \\ \int_{L_1}^{L_2} z \int_0^{2\pi} \frac{1}{(z^2 \tan^2 \omega + (z - Z)^2)^{n+i}} \\ \int_0^1 f_n(r) r^{2i+2} dr d\theta dz = \frac{8\pi^2 a^3 \sin \omega}{\cos^2 \omega} \\ \sum_{i=0}^{\infty} \frac{(n)_i \left(n - \frac{1}{2}\right)_i a^{2i}}{\left(\frac{3}{2}\right)_i i!} \int_0^1 f_n(r) r^{2i+2} dr \\ \int_{L_1}^{L_2} \frac{z}{(z^2 \tan^2 \omega + (z - Z)^2)^{n+i}} dz \quad (35)$$

Next, we solve the integral in z separately from the integral in r .

$$I = \int_{L_1}^{L_2} \frac{z}{(z^2 \tan^2 \omega + (z - Z)^2)^{n+i}} dz \\ = \int_{L_1}^{L_2} \frac{z}{(z^2 \sec^2 \omega - 2zZ + Z^2)^{n+i}} dz \\ = \int_{L_1}^{L_2} \frac{z}{R^{n+i}} dz \quad (36)$$

where $R = \alpha z^2 + \beta z + \gamma$, $\alpha = \sec^2 \omega$, $\beta = -2Z$, and $\gamma = Z^2$. The negative of the discriminant of this quadratic $\Delta = 4\alpha\gamma - \beta^2 = 4Z^2 \sec^2 \omega - 4Z^2 = 4Z^2 \tan^2 \omega$. As the apex angle has valid values $2\omega \in (0, \pi)$, this implies that $\Delta > 0$ for all $Z > 0$. We note that when $Z = 0$ the integral reduces to

$$\cos^{2n+2i} \omega \int_{L_1}^{L_2} z^{1-2n-2i} dz = \cos^{2n+2i} \omega \left[\frac{z^{2-2n-2i}}{2-2n-2i} \right]_{L_1}^{L_2}$$

which does not have any singularities as when $Z = 0$, $L_1 \neq 0$; otherwise the methane molecule and nanocone would be intersecting for all values of $a \geq 0$.

When $Z \neq 0$, we make use of three antiderivatives (eqs 2.171.1, 2.171.4, and 2.172 in ref 44) and then, as there are no singularities in the integrand, we invoke the fundamental theorem of calculus to compute our definite integral:

$$\int x^{m+1} R^n dx = \frac{x^m R^{n+1}}{\alpha(m+2n+2)} - \frac{\gamma m}{\alpha(m+2n+2)} \\ \int x^{m-1} R^n dx - \frac{\beta(m+n+1)}{\alpha(m+2n+2)} \int x^m R^n dx \quad (37)$$

$$\int \frac{dx}{R^{n+1}} = \frac{(2\alpha x + \beta)}{2n+1} \\ \sum_{k=0}^{n-1} \frac{2^k (2n+1)(2n-1)(2n-3)\dots(2n-2k+1)\alpha^k}{n(n-1)\dots(n-k)\Delta^{k+1} R^{n-k}} \\ + 2^n \frac{(2n-1)!! \alpha^n}{n! \Delta^n} \int \frac{dx}{R} = \frac{(2\alpha x + \beta)}{2n+1} \\ \sum_{k=0}^{n-1} \frac{2^k (n-k-1)!! (2n+1)!! \alpha^k}{n! (2n-2k-1)!! \Delta^{k+1} R^{n-k}} + 2^n \frac{(2n-1)!! \alpha^n}{n! \Delta^n} \\ \int \frac{dx}{R} \quad (38)$$

$$\int \frac{dx}{R} = \frac{2}{\sqrt{\Delta}} \arctan\left(\frac{\beta + 2\alpha x}{\sqrt{\Delta}}\right) \quad (\Delta > 0) \quad (39)$$

Taking $m = 0$ and $n = -n - i$, eq 37 becomes the indefinite version of integral I :

$$\int \frac{x}{R^{n+i}} dx = \frac{1}{\alpha(2-2n-2i)R^{n+i-1}} - \frac{\beta(1-n-i)}{\alpha(2-2n-2i)} \\ \int \frac{dx}{R^{n+i}} \quad (40)$$

Combining eqs 38 and 39, we have

$$I(x) = \int \frac{x}{R^{n+i}} dx = \frac{1}{\alpha(2-2n-2i)R^{n+i-1}} \\ - \frac{\beta(1-n-i)}{\alpha(2-2n-2i)} \left(\frac{2\alpha x + \beta}{2(n+i)+1} \right. \\ \left. - \sum_{k=0}^{n+i-1} \frac{2^k (n+i-k-1)!! (2(n+i)+1)!! \alpha^k}{(n+i)!! (2(n+i)-2k-1)!! \Delta^{k+1} R^{n+i-k}} \right. \\ \left. + 2^{n+i} \frac{(2(n+i)-1)!! \alpha^{n+i}}{(n+i)!! \Delta^{n+i}} \frac{2}{\sqrt{\Delta}} \arctan\left(\frac{2\alpha x + \beta}{\sqrt{\Delta}}\right) \right) \quad (41)$$

Thus, we can compute eq 36 as $\int_{L_1}^{L_2} \frac{z}{R^{n+i}} dz = I(L_2) - I(L_1)$. As such, our final result (before the computation of the integral in r) is given by

$$K_n = \frac{8\pi^2 a^3 \sin \omega}{\cos^2 \omega} \sum_{i=0}^{\infty} \frac{\binom{n}{i} \left(n - \frac{1}{2}\right)_i a^{2i}}{\binom{\frac{3}{2}}{i} i!} (I(L_2) - I(L_1)) \int_0^1 f_n(r) r^{2i+2} dr \quad (42)$$

Again, we note that the integral in r is given in the appendix of Stevens et al.³⁶

■ APPENDIX D. MOLECULAR DYNAMICS SIMULATIONS

Large-scale Atomic/Molecular Massively Parallel Simulator (LAMMPS)⁴³ is used in this paper to perform the molecular dynamics simulations for all three systems, namely methane–fullerene, methane–nanotube bundle and methane–open nanocone. All three systems are simulated in a domain of $100 \text{ \AA} \times 100 \text{ \AA} \times 100 \text{ \AA}$. The Lennard-Jones potential is adopted with a cutoff distance of 14 \AA . To compare simulation results with continuum models, we do not simply initialize the interactions and allow the systems to run freely to equilibrium. Instead, the molecules are forced to move relatively to each other in prescribed manners in order to evaluate the potential energy. This method of simulation is identical to a numeric solution of the discrete case of each interaction. In particular, the methane molecule is rotated about its central carbon atom using the command `fix move rotate` in order to avoid configuration bias, while other carbon nanostructures are moved linearly using the `fix move linear` command. In the methane–fullerene system, both methane and fullerene start at the origin and, assuming rotational invariance due to the fullerene being a sphere, the fullerene is moved along the z -axis. In the methane–bundle system, the methane is fixed at the origin and each nanotube is uniformly spaced around the origin, aligned with the z -axis and centered 8 \AA from it. The nanotubes each move linearly away from the origin, maintaining the uniform spacing. Each nanotube is 50 \AA long and situated such that half the length is on either side of the central methane, ensuring that the two ends of the bundle are well beyond the cutoff distance of the simulation. In the methane–open nanocone system, the methane starts on the z -axis at 20 \AA from the apex of the nanocone and the nanocone aligns with the z -axis. The cone then moves along toward the methane molecule during the simulation. Each nanocone has the same radius at L_2 ($\approx 30 \text{ \AA}$), which is much larger than the cutoff distance of the simulation.

■ AUTHOR INFORMATION

Corresponding Author

Kyle Stevens – School of Information and Physical Sciences, University of Newcastle, Callaghan, New South Wales 2308, Australia; orcid.org/0000-0001-8226-9510; Email: kyle.stevens@uon.edu.au

Authors

Ngamta Thamwattana – School of Information and Physical Sciences, University of Newcastle, Callaghan, New South Wales 2308, Australia

Thien Tran-Duc – School of Information and Physical Sciences, University of Newcastle, Callaghan, New South Wales 2308, Australia

Complete contact information is available at:

<https://pubs.acs.org/10.1021/acsomega.2c02485>

Notes

The authors declare no competing financial interest.

■ ACKNOWLEDGMENTS

The authors are grateful for the support of the Australian Research Council through funding of Discovery Project DP170102705.

■ REFERENCES

- (1) Heilig, G. K. The greenhouse gas methane (CH₄): Sources and sinks, the impact of population growth, possible interventions. *Population and environment* **1994**, *16*, 109–137.
- (2) Economides, M. J.; Wood, D. A. The state of natural gas. *J. Nat. Gas Sci. Eng.* **2009**, *1*, 1–13.
- (3) Slugokenky, E. *Carbon Cycle Greenhouse Gases: Trends in Atmospheric CH₄*. Global Monitoring Laboratory. 2005. https://gml.noaa.gov/ccgg/trends_ch4/.
- (4) IPPC. *Climate Change 2021: The Physical Science Basis. Contribution of Working Group I to the Sixth Assessment Report of the Intergovernmental Panel on Climate Change*; Masson-Delmotte, V.; Zhai, P.; Pirani, A.; Connors, S. L.; Péan, C.; Berger, S.; Caud, N.; Chen, Y.; Goldfarb, L.; Gomis, M., et al., Eds.; Cambridge University Press: Cambridge, U.K., 2013.
- (5) Qadir, S.; Gu, Y.; Ali, S.; Li, D.; Zhao, S.; Wang, S.; Xu, H.; Wang, S. A thermally stable isoquinoline based ultra-microporous metal-organic framework for CH₄ separation from coal mine methane. *Chem. Eng. J. (Amsterdam, Neth.)* **2022**, *428*, 131136.
- (6) Tagliabue, M.; Farrusseng, D.; Valencia, S.; Aguado, S.; Ravon, U.; Rizzo, C.; Corma, A.; Mirodatos, C. Natural gas treating by selective adsorption: Material science and chemical engineering interplay. *Chem. Eng. J. (Amsterdam, Neth.)* **2009**, *155*, 553–566.
- (7) Zhang, N.; Pan, Z.; Zhang, Z.; Zhang, W.; Zhang, L.; Baena-Moreno, F. M.; Lichtfouse, E. CO₂ capture from coalbed methane using membranes: a review. *Environ. Chem. Lett.* **2020**, *18*, 79–96.
- (8) Choi, P.-S.; Jeong, J.-M.; Choi, Y.-K.; Kim, M.-S.; Shin, G.-J.; Park, S.-J. A review: methane capture by nanoporous carbon materials for automobiles. *Carbon letters* **2016**, *17*, 18–28.
- (9) Saleman, T. L.; Li, G. K.; Rufford, T. E.; Stanwick, P. L.; Chan, K. I.; Huang, S. H.; May, E. F. Capture of low grade methane from nitrogen gas using dual-reflux pressure swing adsorption. *Chem. Eng. J. (Amsterdam, Neth.)* **2015**, *281*, 739–748.
- (10) Nandanwar, S. U.; Corbin, D. R.; Shiflett, M. B. A review of porous adsorbents for the separation of nitrogen from natural gas. *Ind. Eng. Chem. Res.* **2020**, *59*, 13355–13369.
- (11) He, Y.; Xiang, S.; Zhang, Z.; Xiong, S.; Fronczek, F. R.; Krishna, R.; O'Keeffe, M.; Chen, B. A microporous lanthanide-tricarboxylate framework with the potential for purification of natural gas. *Chem. Commun. (London)* **2012**, *48*, 10856–10858.
- (12) Xu, X.; Zhao, X.; Sun, L.; Liu, X. Adsorption separation of carbon dioxide, methane and nitrogen on monoethanol amine modified β -zeolite. *J. Nat. Gas Chem.* **2009**, *18*, 167–172.
- (13) Rowland, C. A.; Lorzing, G. R.; Gosselin, A. J.; Trump, B. A.; Yap, G. P.; Brown, C. M.; Bloch, E. D. Methane storage in paddlewheel-based porous coordination cages. *J. Am. Chem. Soc.* **2018**, *140*, 11153–11157.
- (14) Yan, Y.; Kolokolov, D. I.; Da Silva, I.; Stepanov, A. G.; Blake, A. J.; Dally, A.; Manuel, P.; Tang, C. C.; Yang, S.; Schroder, M. Porous metal-organic polyhedral frameworks with optimal molecular dynamics and pore geometry for methane storage. *J. Am. Chem. Soc.* **2017**, *139*, 13349–13360.

- (15) Simon, C. M.; Kim, J.; Gomez-Gualdrón, D. A.; Camp, J. S.; Chung, Y. G.; Martin, R. L.; Mercado, R.; Deem, M. W.; Gunter, D.; Haranczyk, M.; et al. The materials genome in action: identifying the performance limits for methane storage. *Energy Environ. Sci.* **2015**, *8*, 1190–1199.
- (16) Casco, M. E.; Martínez-Escandell, M.; Gadea-Ramos, E.; Kaneko, K.; Silvestre-Albero, J.; Rodríguez-Reinoso, F. High-pressure methane storage in porous materials: are carbon materials in the pole position? *Chem. Mater.* **2015**, *27*, 959–964.
- (17) Peng, Y.; Krungleviciute, V.; Eryazici, I.; Hupp, J. T.; Farha, O. K.; Yildirim, T. Methane storage in metal–organic frameworks: current records, surprise findings, and challenges. *J. Am. Chem. Soc.* **2013**, *135*, 11887–11894.
- (18) Ben, T.; Pei, C.; Zhang, D.; Xu, J.; Deng, F.; Jing, X.; Qiu, S. Gas storage in porous aromatic frameworks (PAFs). *Energy Environ. Sci.* **2011**, *4*, 3991–3999.
- (19) Furukawa, H.; Yaghi, O. M. Storage of hydrogen, methane, and carbon dioxide in highly porous covalent organic frameworks for clean energy applications. *J. Am. Chem. Soc.* **2009**, *131*, 8875–8883.
- (20) Kemp, K. C.; Baek, S. B.; Lee, W.-G.; Meyyappan, M.; Kim, K. S. Activated carbon derived from waste coffee grounds for stable methane storage. *Nanotechnology* **2015**, *26*, 385602.
- (21) Antoniou, M. K.; Diamanti, E. K.; Enotiadis, A.; Policicchio, A.; Dimos, K.; Ciuchi, F.; Maccallini, E.; Gournis, D.; Agostino, R. G. Methane storage in zeolite-like carbon materials. *Microporous Mesoporous Mater.* **2014**, *188*, 16–22.
- (22) Kowalczyk, P.; Solarz, L.; Do, D.; Samborski, A.; MacElroy, J. Nanoscale tubular vessels for storage of methane at ambient temperatures. *Langmuir* **2006**, *22*, 9035–9040.
- (23) Bekyarova, E.; Murata, K.; Yudasaka, M.; Kasuya, D.; Iijima, S.; Tanaka, H.; Kahoh, H.; Kaneko, K. Single-wall nanostructured carbon for methane storage. *J. Phys. Chem. B* **2003**, *107*, 4681–4684.
- (24) Cychosz, K. A.; Thommes, M. Progress in the physisorption characterization of nanoporous gas storage materials. *Engineering* **2018**, *4*, 559–566.
- (25) Feroldi, M.; Neves, A.; Borba, C.; Alves, H. Methane storage in activated carbon at low pressure under different temperatures and flow rates of charge. *J. Cleaner Prod.* **2018**, *172*, 921–926.
- (26) Thornton, A. W. *Mathematical Modelling of Gas Separation and Storage Using Advanced Materials*. Ph.D. Thesis, University of Wollongong, 2009.
- (27) Jones, J. E. On the determination of molecular fields.—I. From the variation of the viscosity of a gas with temperature. *Proc. R. Soc. A* **1924**, *106*, 441–462.
- (28) Girifalco, L. A. Molecular properties of fullerene in the gas and solid phases. *J. Phys. Chem.* **1992**, *96*, 858–861.
- (29) Baowan, D.; Cox, B. J.; Hilder, T. A.; Hill, J. M.; Thamwattana, N. *Modelling and Mechanics of Carbon-Based Nanostructured Materials*, 1st ed.; William Andrew: 2017; pp 1–89.
- (30) Cox, B. J.; Thamwattana, N.; Hill, J. M. Mechanics of atoms and fullerenes in single-walled carbon nanotubes. I. Acceptance and suction energies. *Proc. R. Soc. A* **2007**, *463*, 461–477.
- (31) Tran-Duc, T.; Thamwattana, N.; Cox, B. J.; Hill, J. M. Adsorption of polycyclic aromatic hydrocarbons on graphite surfaces. *Comput. Mater. Sci.* **2010**, *49*, S307–S312.
- (32) Ansari, R.; Sadeghi, F.; Mottevalli, B. A comprehensive study on the oscillation frequency of spherical fullerenes in carbon nanotubes under different system parameters. *Communications in Nonlinear Science and Numerical Simulation* **2013**, *18*, 769–784.
- (33) Rajabi, K.; Hosseini-Hashemi, S. Effect of the interparticle interactions on adsorption-induced frequency shift of nano-beam-based nanoscale mass-sensors: A Theoretical study. *J. Solid Mech.* **2018**, *10*, 864–873.
- (34) Pogorelov, E. G.; Zhbanov, A. I.; Chang, Y.-C.; Yang, S. Universal curves for the van der Waals interaction between single-walled carbon nanotubes. *Langmuir* **2012**, *28*, 1276–1282.
- (35) Ghavanloo, E.; Fazelzadeh, S. A. Continuum modeling of breathing-like modes of spherical carbon onions. *Phys. Lett. A* **2015**, *379*, 1600–1606.
- (36) Stevens, K.; Thamwattana, N.; Tran-Duc, T. New functional Lennard-Jones parameters for heterogeneous molecules. *J. Appl. Phys.* **2020**, *128*, 204301.
- (37) Stevens, K.; Tran-Duc, T.; Thamwattana, N.; Hill, J. M. Modeling Interactions between Graphene and Heterogeneous Molecules. *Computation* **2020**, *8*, 107.
- (38) Tran-Duc, T.; Thamwattana, N.; Cox, B. J.; Hill, J. M. Modelling the interaction in a benzene dimer. *Philos. Mag.* **2010**, *90*, 1771–1785.
- (39) Adisa, O. O.; Cox, B. J.; Hill, J. M. Encapsulation of methane molecules into carbon nanotubes. *Phys. B (Amsterdam, Neth.)* **2011**, *406*, 88–93.
- (40) Adisa, O. O.; Cox, B. J.; Hill, J. M. Encapsulation of methane in nanotube bundles. *Micro Nano Lett.* **2010**, *5*, 291–295.
- (41) Adisa, O. O.; Cox, B. J.; Hill, J. M. Methane storage in spherical fullerenes. *J. Nanotechnol. Eng. Med.* **2012**, *3*, 041002.
- (42) Adisa, O. O.; Cox, B. J.; Hill, J. M. Open carbon nanocones as candidates for gas storage. *J. Phys. Chem. C* **2011**, *115*, 24528–24533.
- (43) Thompson, A. P.; Aktulga, H. M.; Berger, R.; Bolintineanu, D. S.; Brown, W. M.; Crozier, P. S.; in 't Veld, P. J.; Kohlmeyer, A.; Moore, S. G.; Nguyen, T. D.; Shan, R.; Stevens, M. J.; Tranchida, J.; Trott, C.; Plimpton, S. J. LAMMPS - a flexible simulation tool for particle-based materials modeling at the atomic, meso, and continuum scales. *Comput. Phys. Commun.* **2022**, *271*, 108171.
- (44) Gradshteyn, I. S.; Ryzhik, I. M. *Table of Integrals, Series, and Products*, 8th ed.; Academic Press: 2014.